AN EFFICIENT SEA LEVEL MONITORING SOLUTION BY BLENDING HIMAWARI-8 AND LANDSAT IMAGERY

Andriani Putri[1] and Chih-Yuan Huang[2]
[1]Center for Space and Remote Sensing Research, National Central University,
No. 300, Zhongda Rd, Zhongli District, Taoyuan City 32001, Taiwan (R.O.C)
Email: andrianip92@g.ncu.edu.tw
[2]Center for Space and Remote Sensing Research, National Central University,
No. 300, Zhongda Rd, Zhongli District, Taoyuan City 32001, Taiwan (R.O.C)
Email: cyhuang@csrsr.ncu.edu.tw

KEY WORDS: Spatial-temporal image fusion, STARFM, Himawari-8, Landsat-8, water level monitoring

ABSTRACT: High spatial and temporal resolutions of satellite imagery are necessary for improving the ability to monitor rapid environment changes at finer scales. However, no single satellite can produce images with both high spatial and temporal resolutions. To address this issue, spatio-temporal fusion algorithms, such as the Spatial and Temporal Adaptive Reflectance Fusion Model (STARFM) was proposed to synthesize high spatial and temporal resolution images. On the other hand, water level monitoring is important to support natural hazard management, such as floods and tsunamis. However, continuously monitoring these hazards are challenging for a remote sensing satellite due to either its low spatial resolution or low temporal resolution. For example, Operational Land Imager (OLI) onboard Landsat 8 with a spatial resolution of 30 m has been applied on water level detection, but it cannot capture dynamic events due to its low temporal resolution. On the other hand, The Advanced Himawari Imager (AHI) 8 only needs 10 minutes to watch the hemisphere once, but its coarse resolution hampers the accurate mapping of sea level change. This study, therefore, aims to blend Landsat OLI imagery with Himawari-8 imagery to monitor the dynamic and local behavior of sea level changes. To be specific, we first calculate the modified Normalized Difference Water Index (mNDWI) using Landsat and Himawari-8 images and then fuse the index images using the STARFM algorithm. Finally, the water coverage is delineated by setting a threshold on the mNDWI index. By comparing the retrieved water coverage percentage with in-situ water level observations, we have seen a promising result.

1. INTRODUCTION

Recent improvements of remote sensing allow for the acquisition of high-resolution images to be used in wide variety of applications, such as in urban planning, forestry management, and water surface mapping. As the remote sensing is getting common to be used in many fields, high spatial and temporal resolution of satellite imagery are necessary for improving the ability to monitor the change of environment at finder scales. However, no single satellite can produce images with both high spatial and temporal resolutions. This kind of problem can be a big issue while sensors will be applied in applications that needs these both high resolutions. One of these applications is in monitoring sea level change (Kostiuk, 2002). Sea level is the average height of the ocean's surface between high and low tides. Sea level rise not only causes floods but also contaminates fresh water and harms coastal ecosystems. Hence, sea level monitoring is necessary for disaster management and avoidance.

Various remote sensors have been applied in detecting and monitoring surface water since the 1970s, such as Moderate Resolution Imaging Spectroradiometer (MODIS), and Suomi National Polar-orbiting Partnership - Visible Infrared Imaging Radiometer Suite (NPP-VIIRS). Earth observation satellites, such as Landsat and Himawari-8, provide data at different spatial, temporal and spectral resolutions. For example, the fine-resolution sensor, Operational Land Imager (OLI) onboard Landsat 8 with a spatial resolution of 30 m is considered a continuation of the Landsat series. Its applicability in seawater detection has been tested (Moradi et al., 2016), but it cannot capture the dynamic changes of seawater as it has a low temporal resolution of 16 days. On the other hand, the coarse-resolution sensor, the Advanced Himawari Imager (AHI) 8 provides a high temporal resolution which only needs 10 minutes to watch the hemisphere once. Including the aforementioned remote sensors that have been applied for seawater detection, however, no single satellite can provide imagery with both high spatial and temporal resolutions.

To overcome this well-known issue in remote sensing, fusing data from different sensors has gained increasing popularity in recent years by combining high temporal resolution sensors such as AHI with medium to high spatial resolution sensor like Landsat OLI data. As shown in Table 1, the bandwidths of these two sensors are similar which makes the image fusion possible. In this paper, we use hourly Himawari-8 surface reflectance and blend with Landsat OLI images to achieve efficient sea level monitoring.

Table 1. Corresponding bands list of Landsat OLI and Himawari-8

Spectral Region	Band		Wavelength (μm)		Spatial Resolution (m)	
	Landsat OLI	Himawari-8	Landsat OLI	Himawari -8	Landsat OLI	Himawari-8
Ultra Blue	1	-	0.43 - 0.45	-	30	-
Blue	2	1	0.45 - 0.51	0.47	30	1000
Green	3	2	0.53 - 0.59	0.51	30	500
Red	4	3	0.64 - 0.67	0.64	30	1000
NIR	5	4	0.85 - 0.88	0.86	30	2000
SWIR 1	6	5	1.57 - 1.65	1.61	30	2000
SWIR 2	7	6	2.11 - 2.29	2.23	30	2000

2. RELATED WORK

Image fusion is a remote sensing technique that has been applied to obtain more information by integrating images from different sensors. In general, image fusion algorithms can be divided into two categories. The first category, spatial-spectral image fusion, or known as pan-sharpening, blends a lower resolution multispectral image with a higher resolution panchromatic image (Dhore & Veena, 2014). Many studies focused on the fusing of a fine resolution panchromatic band and coarse resolution spectral bands from one or more sensors. But however, the outputs from those techniques were not calibrated to spectral radiance or reflectance. The traditional data fusing approaches such as those using hue saturation value (HSV) transforms (Al-Wassai et al., 2011), principal component analysis (Metwalli et al., 2009) and wavelet transformation (Pajares & Cruz, 2004) may not suitable for the problem considered here, since we wish to capture the high frequency sea level change based on the surface reflectance.

The second category, spatial-temporal image fusion aims at blending high spatial resolution data with high temporal resolution data to achieve both high spatial and high temporal resolutions. The spatial-temporal image fusion has been proven to be an effective solution for different spatial and temporal sensors. Wu et al. (2015) presented a spatial-temporal image fusion model to blend multi-sources of remotely sensed data to achieve both higher spatial and temporal resolutions of land surface temperature observation. Gao et al. (2006) proposed the Spatial and Temporal Adaptive Reflectance Fusion Model (STARFM) to generate a daily synthetic Landsat-like image by blending Landsat and MODIS images. Another image fusion model is for producing synthetic imagery and the detection of changes termed Spatial-Temporal Adaptive Algorithm for mapping Reflectance Change (STAARCH) (Hilker et al., 2009). The algorithm is designed to detect changes in reflectance, denoting disturbance, using Tasseled Cap transformations of both Landsat TM/ETM and MODIS reflectance data. STAARCH also includes functionality for estimating surface reflectance, based on an extended version of STARFM. Zhu et al. (2010) later modified the original STARFM as Enhanced STARFM (ESTARFM), which improves the prediction in complex heterogeneous regions by involving additional input images. However, because of the simplicity of the STARFM, this research chooses the STARFM as the spatial-temporal image fusion algorithm.

In STARFM, the coarse resolution data are first reprojected and resampled to match with the fine resolution imagery. Then an unsupervised classification is employed to classify the land cover from the image to identify pixels that are spectrally similar. Both fine- and coarse-resolution data are then used to determine the weights for the image fusion process, which is shown in the following equation.

$$F\left(x_{\frac{w}{2}}, y_{\frac{w}{2}}, t_0\right) = \sum_{i=1}^{w} \sum_{j=1}^{w} \sum_{k=1}^{n} W_{ijk} * \left(L\left(x_i, y_j, t_0\right) + F\left(x_i, y_j, t_k\right) - L\left(x_i, y_j, t_k\right)\right)$$

where w is the searching window size and $(x_{w/2}, y_{w/2})$ is the central pixel of a moving window. F and L represent fine- and low- resolution images, respectively. t_k and t_0 represent the time-points of reference data and prediction data, respectively. W is a combined weighting based on spectral, temporal, and distance information. To ensure that the right information from neighbor pixels is used, only spectrally similar and cloud-free pixels from Landsat surface reflectance within the moving window are used. Finally, the prediction value is computed from these weighted values.

3. METHODOLOGY

This study aims at monitoring the dynamic changes of sea level using the STARFM by blending two satellites imagery from different sensors, the Advanced Himawari Imager and Landsat 8. To be specific, first, all the images in the testing area, the coastline of Kaohsiung Port as shown in Figure 1, should be calibrated to surface reflectance and co-registered (via affine transformation). After that, with the Green and SWIR bands, we can calculate the modified Normalized Different Water Index (mNDWI) from Himawari and Landsat images, which is an effective indicator of water region (Xu, 2006). To delineate water and non-water area, a manually-selected mNDWI threshold value of 0.4 was applied.

As the input of the STARFM, the Himawari and Landsat images at reference date along with the classification maps from Landsat at the predicted date were used. All the input images of the STARFM are in water index values, this approach corresponds to the Index-then-Blend approach mentioned in (Jarihani et al., 2014). Using the classification maps of the various sea water level to predict the sea level on the certain date or time. The classification map is used as the input of STARFM and applied along with the Landsat image at the reference date and also the Himawari-8 image. The classification map is derived by k-means unsupervised classification which is one of the common classification methods.

In this study, we evaluate the result from two perspectives. Firstly, the spatial evaluation analyzes the accuracy of the retrieved water region by comparing with the water region retrieved from actual Landsat images. Secondly, the temporal evaluation compares the trend of water region changes retrieved from predicted images with the in-situ water level observations. The in-situ data was collected from the Central Weather Bureau in Taiwan. The hourly images of Himawari-8 at 09.00 a.m. to 03.00 p.m. are used as the inputs to predict 30 meters resolution images at 09.00 a.m. to 03.00 p.m.

For the spatial evaluation, the high-resolution image on 2 April 2017 is predicted with the reference image of Landsat and Himawari-8 on 1 March 2017 and the Himawari-8 image at the predict date. The actual Landsat mNDWI image at 2 April was employed to calculate the Overall Accuracy, Kappa Coefficient, Commission and Omission Errors. In terms of the temporal evaluation, as the water level changes dynamically, the classification maps for fusing images at different time points should be corresponding to the water height at those time points. To achieve this, this research applies a coarse-to-fine solution. We first apply an existing tide model called NAO.99b to derive a candidate water height at the predict time, and then use the candidate water height to find a suitable reference data for image fusion, including cloud-free Landsat and AHI images and the classification map from that Landsat image. For this preliminary study, we collect three nearly cloud-free Landsat images and their corresponding water height, as shown in Table 2.

Table 2. Reference Landsat image list and the corresponding water height

Date	Time	Water Height (m)
2017/Jan/12	10.30 a.m.	-0.131
2017/Mar/01	10.30 a.m.	0.256
2017/Apr/02	10.30 a.m.	0.481

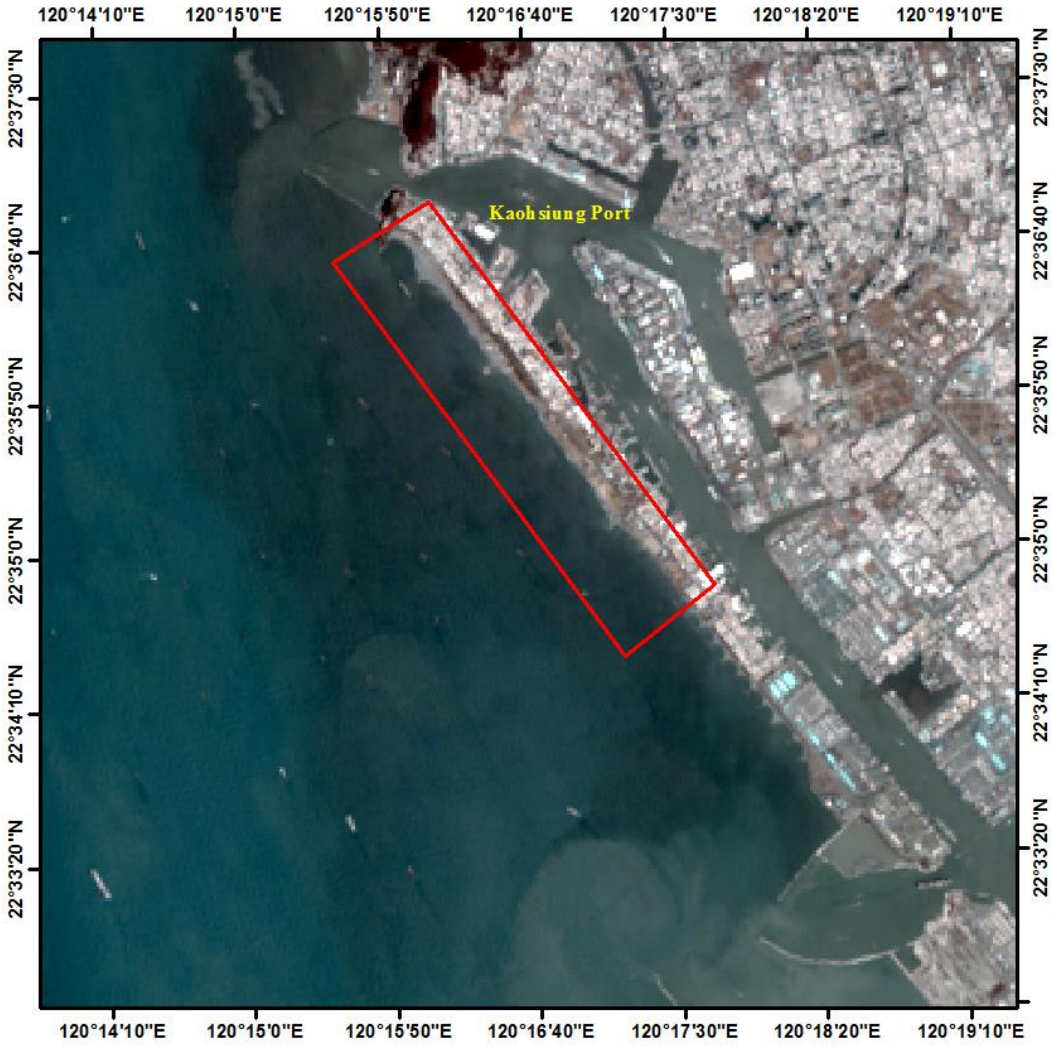

Figure 1. Testing area displayed as Landsat Imagery bands (R4G3B2)

Then hourly Himawari-8 images on 01 March 2017 at 09.00 a.m. to 03.00 p.m. were prepared and also the water height of each hour was derived from the tide model. The following table shows the hourly water height on 01 March 2017 that will be used to select the reference images.

Table 3. Time points of Himawari-8 and the water height at each hour

Time	Water Height (m)
09.00 a.m.	0.24
10.00 a.m.	0.278
11.00 a.m.	0.234
12.00 p.m.	0.121
01.00 p.m.	-0.032
02.00 p.m.	-0.184
03.00 p.m.	-0.295

After deriving all the information above, then we pair each Himawari-8 water height to the water height of reference Landsat images. If the water heights between Landsat and Himawari-8 are closely similar, a Landsat image will be chosen as the reference for image fusion, as shown in the following table.

Table 4. The pair of Himawari-8 and Classification map used

Pair number	Himawari-8 image	Selected reference Landsat image
#1	09.00 a.m.	2017/Mar/01
#2	10.00 a.m.	2017/Mar/01
#3	11.00 a.m.	2017/Mar/01
#4	12.00 p.m.	2017/Mar/01
#5	01.00 p.m.	2017/Jan/12
#6	02.00 p.m.	2017/Jan/12
#7	03.00 p.m.	2017/Jan/12

To be specific, for number #1 at 09.00 a.m., the reference data for image fusion are the Himawari-8 and Landsat images at 10.30 a.m. on 01 March 2017 along with the corresponding classification map. The Himawari-8 image at predicted time, 09.00 a.m. on 01 March 2017, is used as the coarse-resolution image at the predicted time. Please also note that currently, the database for the reference data is still very preliminary. One of our main future work is to expand that database to find a better corresponding reference data for different water heights.

4. PRELIMINARY RESULTS

Validation mainly involves two aspects in this study. On is the spatial evaluation which evaluate the accuracy of sea water mapping, and the other is comparing the result of retrieved water region with in-situ water level observations.

4.1 Spatial Evaluation

Figure 2 shows the reference images used to predict high resolution image on 02 April 2017 (Figure 2d). Figure (2a) shows the reference mNDWI image from Himawari-8 on 1 March 2017 and the Landsat image at reference date (Figure 2c). To predict the image on predict date, the image of Himawari-8 at the on the predict date is used (Figure 2c).

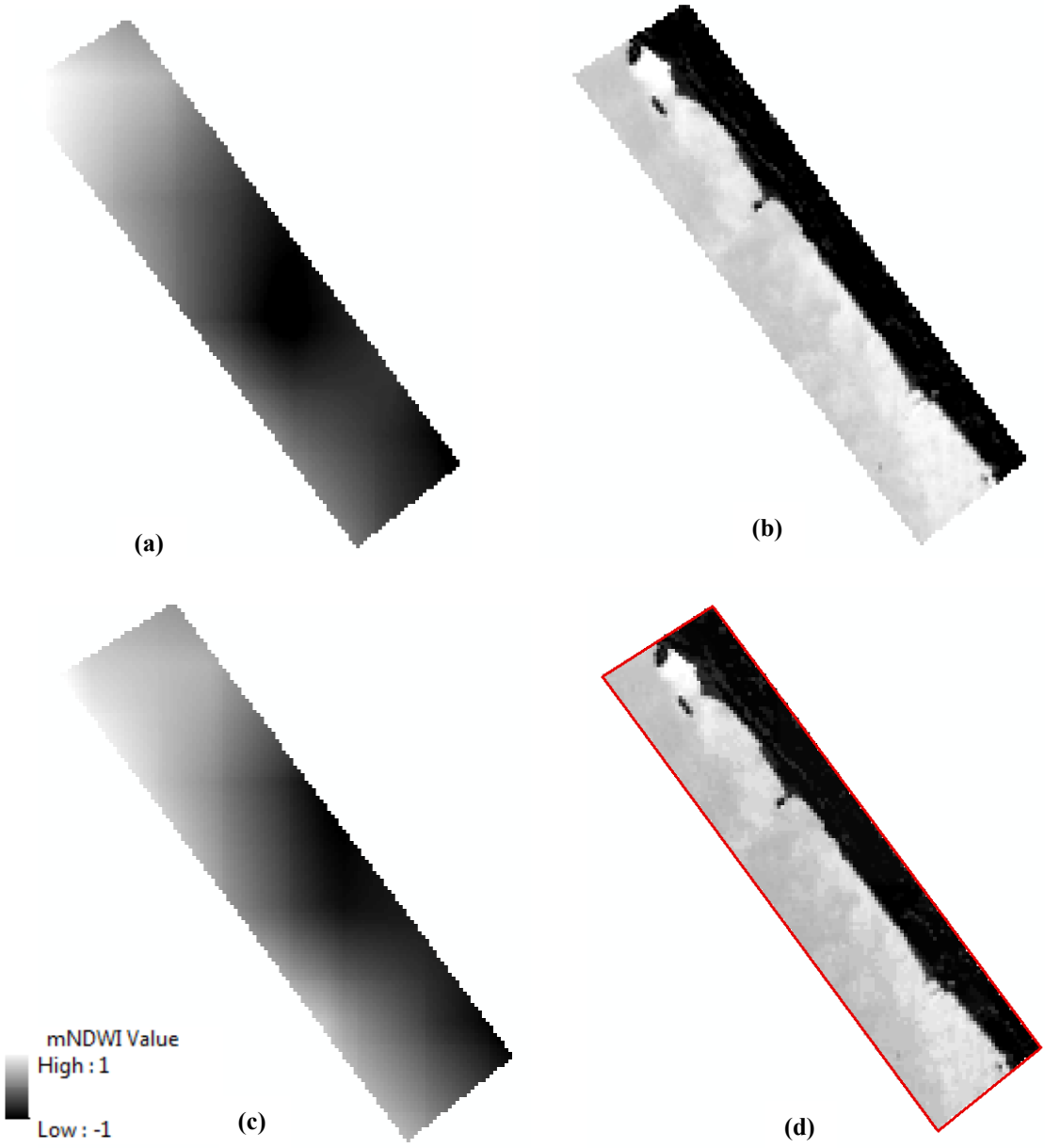

Figure 2. (a) reference mNDWI image derived from Himawari-8 on 1 March 2017; (b) reference mNDWI image derived from Landsat on 1 March 2017; (c) mNDWI image derived from Himawari-8 on predicted date 2 April 2017; (d) the predicted image on 2 April 2017.

An actual Landsat image was employed to validate the results of STARFM, as shown in Figure 3. Water map of the predicted result was overlaid with the reference Landsat water map on a pixel-by-pixel basis and an evaluation map was produced (Figure 4). Misclassified water areas can be easily identified from the map. It is observed that the errors in the water map comes from the underestimates of water area which reflects to the omission errors.

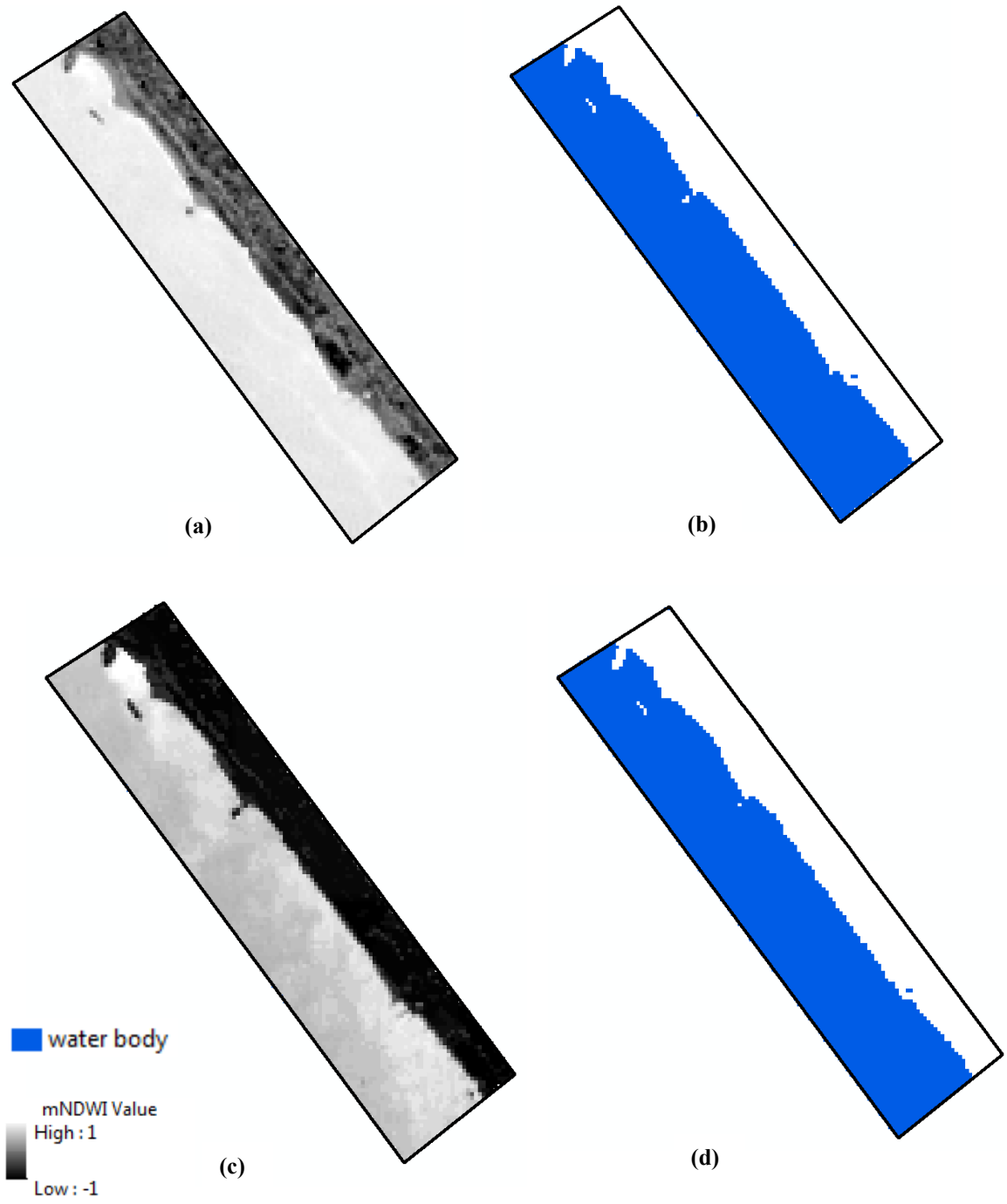

Figure 3. (a) mNDWI image derived from the actual Landsat image at 10.30 a.m on 02 April 2017; (b) water map derived from the actual Landsat 10.30 a.m on 02 April 2017; (c) mNDWI image derived from predicted image result; (c) water map derived from predicted image result.

Commonly-used accuracy evaluation indices, including commission and omission errors, overall accuracy and Kappa coefficient, were calculated from evaluation map of Figure 4, and listed in Table 5. This table provides a more straightforward comparison on the results of predicted image. High value in Kappa and overall accuracy indicate the general consistency between the predicted map of the predicted image and the reference map of actual Landsat image. However, there are some omission error occurs at the coastal region, which we think is because the water height of the reference data (0.256 m) is lower than the water height of the predicted time (0.481 m).

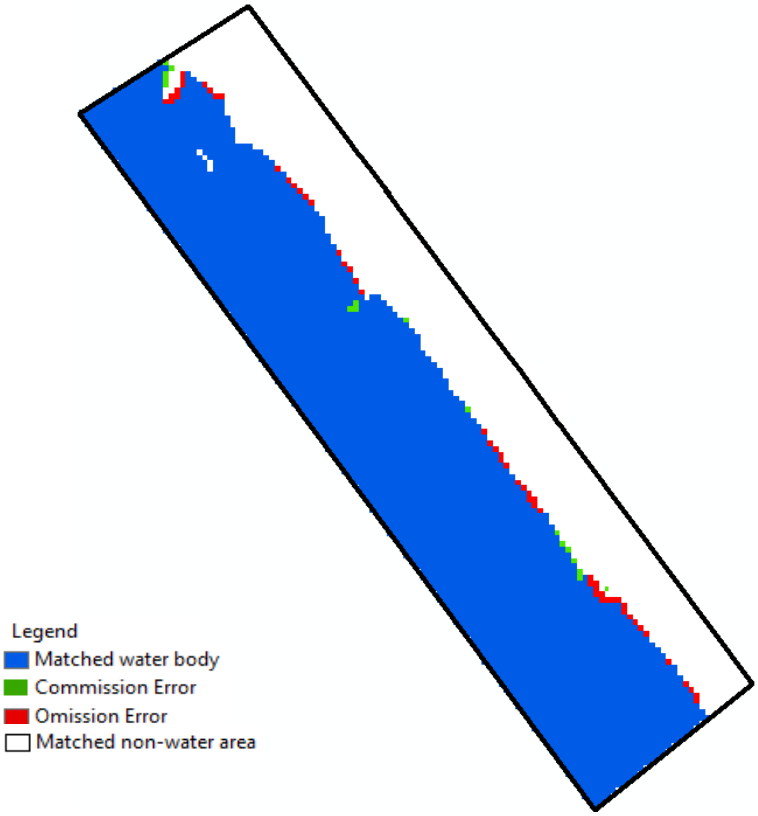

Figure 4. Evaluation map of the predicted result

Table 5. Accuracy of spatial evaluation results

Commission Error (%)	Omission Error (%)	Overall Accuracy (%)	Kappa Coefficient
1.07	2.77	96	0.92

4.2 Temporal Evaluation

For the temporal evaluation, we compare the hourly water coverage percentages retrieved from fused images with the water heights from the in-situ observations. The comparison is shown in Figure 5. In principle, the higher water level should have larger water coverage.

Figure 5 shows that the overall trend of the water coverage and the water height fit with each other. However, there are still some small errors, which we believe the main reason is that the classification maps used for the predicate time do not have the corresponding weight height. For example, the water height at 03.00 p.m. is -0.295 m, but the selected reference data is at -0.131 m. We believe that once the database for the reference data is extended to cover the possible water heights, the image fusion result can be further improved.

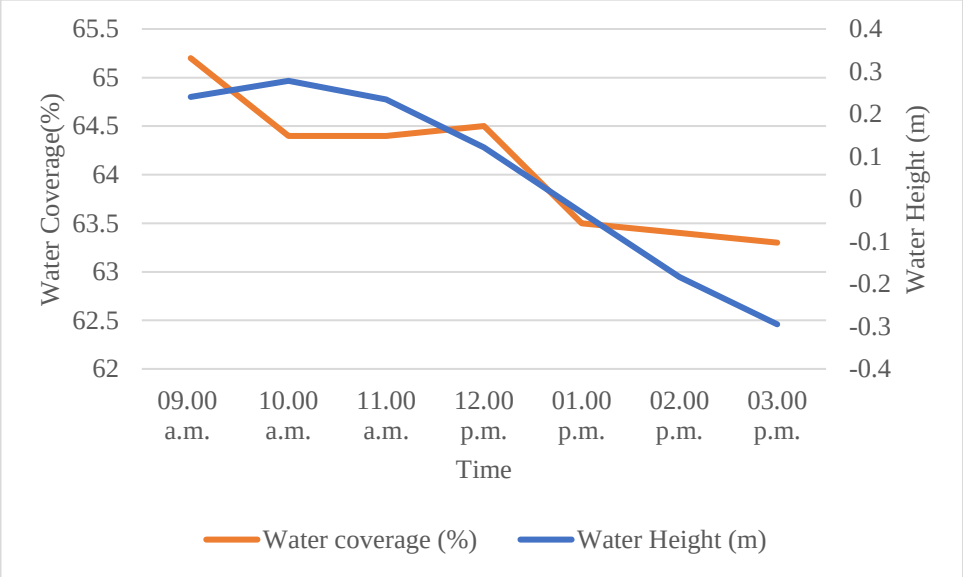

Figure 5. Temporal evaluation result

5. CONCLUSIONS AND FUTURE WORK

Monitoring sea level change requires both high spatial and high temporal resolutions, especially for avoiding hazards such as flood and tsunami. Unfortunately, no single remote sensor has both high spatial and high temporal resolutions. This study examines the feasibility of an existing image fusion model, the STARFM, in blending Landsat and Himawari-8 images for the sea level monitoring. The evaluations show that STARFM can successfully fuse Landsat and Himawari-8 images. Both the spatial evaluation and the temporal evaluation shows convincing result. However, we can also observe that the selection of corresponding classification maps is a crucial factor. Hence, one of the immediate next steps of this study is to collect more Landsat images to provide more choices for the water height reference data. In addition, more testing data and testing sites will be examined for a more comprehensive evaluation.

REFERENCE

Al-Wassai, F.A.; Kalyankar, N.V.; Al-Zuky, A.A., 2011. The HIS Transformations Based Image Fusion. Computer Vision and Pattern Recognition(cs.CV), pp. 1-10.

Dhore, A.; Veena.; 2014. A New Pan-sharpening Method Using Joint Sparse FI Image Fusion Algorithm. International Journal of Engineering Research and General Science. pp. 447-455.

Gao, F.; Masek, J.; Schwaller, M.; Hall, F., 2006. On the blending of Landsat and MODIS surface reflectance: Predicting daily Landsat surface reflectance. IEEE Transactions on Geoscience and Remote Sensing, pp. 2207-2218.

Hilker, T., Wulder, M.A., Coops, N.C., Linke, J., McDermid, G., Mae, J.F., Gao, F., White, J.C., 2009. A new data fusion model for high spatial-and temporal-resolution mapping of forest disturbance based on Landsat and MODIS. Remote Sensing of Environment., pp. 1613-1627.

Jarihani, A.A.; McVicar, T.R.; Van Niel, T.G.; Emelyanova, I.V.; Callow, J.N.; Johansen, K., 2014. Blending Landsat and MODIS Data to Generate Multispectral Indices: A Comparison of "Index-then-Blend" and "Blend-then-Index" Approaches. Remote Sens., pp. 9213–9238.

Kostiuk, M., 2002. Using Remote Sensing Data to Detect Sea Level Change. Pecora 15, pp. 1-9.

Metwalli, M.R.; Nasr A.H.; Allah O.S.F.; El-Rabaie, S., 2009. Image Fusion Based on Principal Component Analysis and High-Pass Filter. IEEE, pp. 63-70.

Pajares, G.; Cruz, J.M. de la., 2004. A wavelet-based Image Fusion Tutorial. Elsevier. pp. 1855-1872.

Xu, H.Q., 2006. Modification of normalised difference water index (NDWI) to enhance open water features in remotely sensed imagery, Int. J. Remote Sens., pp. 3025-3033.

Zhu, X.; Chen, J.; Gao, F.; Chen, X.; Masek, J., 2010. An enhanced spatial and temporal adaptive reflectance fusion model for complex heterogeneous regions. Remote Sens. Environ., pp. 2610-2623.